

Cite this: *Soft Matter*, 2012, **8**, 8464

www.rsc.org/softmatter

PAPER

Morphology and rheology of ternary fluid–fluid–solid systems†

Shailesh P. Nagarkar and Sachin S. Velankar*

Received 1st April 2012, Accepted 21st June 2012

DOI: 10.1039/c2sm25758k

We examine the effects of interfacially active particles in blends of immiscible homopolymers with a droplet/matrix morphology. The effect of particles on drop size is not monotonic: at low volume fractions ($\sim 0.1\%$), particles greatly increase the size of the dispersed phase by promoting flow-induced coalescence regardless of which phase wets the particles preferentially. At higher particle loadings (~ 1 vol%), the particles completely cover the interface and reduce the size of the dispersed phase. Particles that are preferentially wetted by the continuous phase are also able to glue together two drops by bridging across them. In this case the morphology consists of clusters of particle-bridged drops, and the resulting blends show solid-like rheology. At low particle loadings, most of the particles are sandwiched between drops, leaving the rest of the interface particle-free. At high particle loadings, the entire surface is nearly covered with particles, the drops are faceted, and the morphology resembles a foam structure. In contrast to these results, particles that are preferentially wetted by the dispersed phase or equally wetted by both phases are not capable of bridging, and these blends do not show drop clusters. These results offer new insights on the behavior of ternary systems composed of two fluids and one particulate species.

1. Introduction

Solid particles that are partially wetted by two immiscible fluid phases can adsorb at the interface between the two fluids, as shown in Fig. 1A. Such interfacially adsorbed particles are somewhat analogous to amphiphilic molecular surfactants.¹ Like surfactants, such interfacially adsorbed particles can stabilize emulsions, commonly known as Pickering emulsions.^{1–3} Particle-induced interfacial stabilization can also be exploited in gas–liquid systems to fabricate foams^{4,5} or “dry liquids”.^{6,7} Beyond stabilizing multiphase fluid systems however, particles can greatly affect the morphology of two-phase liquid–liquid systems. For example, if particles added to a droplet/matrix

morphology adsorb at the interface to a sufficiently high surface coverage, they can jam the interface and give rise to non-spherical drop shapes.^{2,8,9} Similar jamming in bicontinuous two-phase morphologies can arrest structural coarsening and yield “bijels”, *i.e.* bicontinuous interfacially jammed emulsions.^{10–14} Yet another remarkable phenomenon is “bridging” in which a single particle can simultaneously adsorb on two drops, and stabilize the thin film of continuous-phase fluid separating the drops as shown in Fig. 1B.^{15–17} When this occurs, the drops are glued together: they cannot separate readily, but nor can they coalesce, leading to a new mechanism of emulsion stabilization.^{18–22} Interfacial jamming and particle-bridging is expected to cause profound changes in structure, stability, and rheological properties of multiphase fluid systems. Fig. 2 illustrates the ternary composition diagram for a mixture of two fluids and one particulate species and lists some of the morphologies that have already been found, nevertheless, much of this parameter space remains unexplored. Many questions, *e.g.* effects of particle wettability, size, or stress, on the structure and flow properties of the ternary systems remain poorly understood. Most importantly, the morphology of these ternary systems is determined not by equilibrium thermodynamics, but by the specific processing history, and there is little information about how processing history affects the structure and flow properties.

One reason for this lack of knowledge is the difficulty of structural characterization at the particle scale. Most of the past research on interfacial adsorption of particles has been performed using oil–water or air–water systems. Such systems present a significant challenge for fundamental studies, chiefly

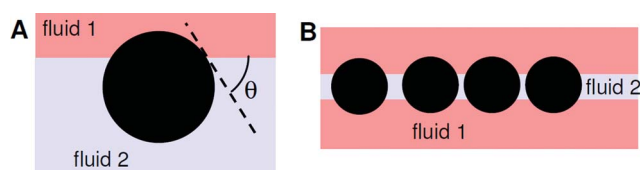


Fig. 1 (A) A particle adsorbed at the interface between two fluids. Here $\theta < 90^\circ$ indicates that the particle is preferentially wetted by the fluid 2. (B) A monolayer of particles, each adsorbed at two fluid–fluid interfaces. Figure is color online.

Dept. of Chemical Engineering, University of Pittsburgh, Pittsburgh PA 15261, USA. E-mail: velankar@pitt.edu

† Electronic supplementary information (ESI) available. See DOI: 10.1039/c2sm25758k

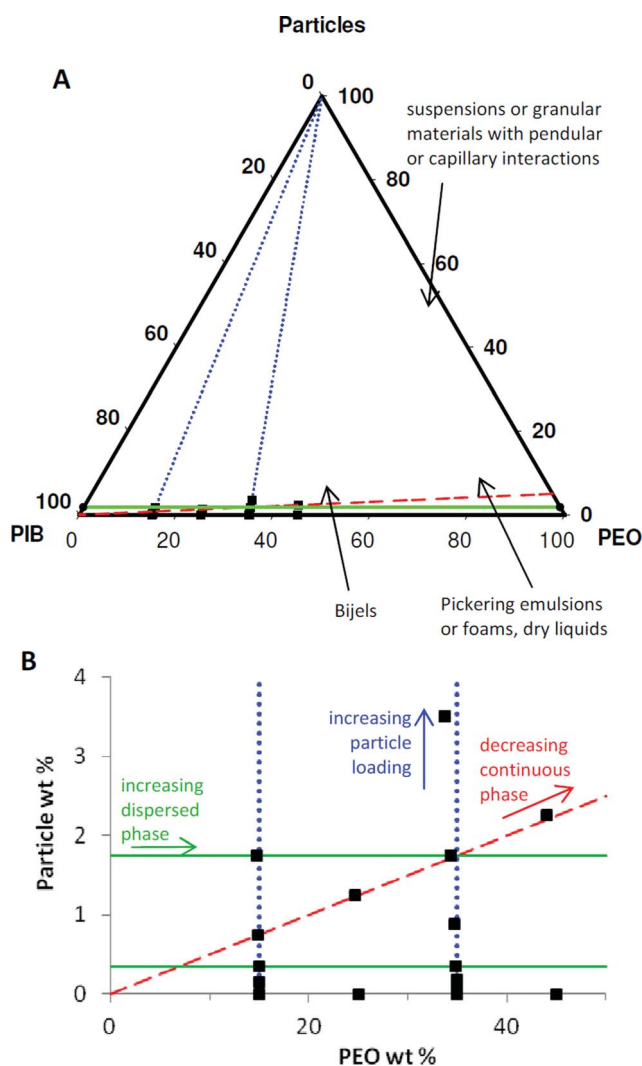


Fig. 2 (A) Ternary composition diagram for a mixture of two liquids (in the present case PEO and PIB), and solid particles. The filled symbols correspond to the compositions studied in this paper which are all at low particle loadings. Bijels occur near equal volume ratios of the two liquids.^{10–14} Pickering emulsions occur when one fluid is in a majority.¹ Particle-stabilized foams occur when particles coat air bubbles in a continuous phase liquid.^{4,5} Dry liquids occur when particles coat liquid drops in air.^{6,7} Suspensions or granules with pendular (or capillary) interactions correspond to a high particle loading, with a small amount of particle-wetting (or particle-non-wetting) liquid.^{57,59,65} (B) Magnified view of the region of composition space examined here. In this region, the Cartesian plot shown is a good approximation of the actual triangular composition diagram. Figure is color online.

because since the components are liquid at room temperature, structural information at the scale of particles, which are often sub-micron sized, is difficult to obtain. The challenge is compounded by the fact that since the morphology is not at equilibrium, it must be characterized with minimal disturbance. Optical microscopy or confocal imaging can characterize the two-phase morphology, provided light scattering is not too severe, *i.e.* if the samples are thin or the refractive index of both fluids and the particles are nearly equal.^{12,23,24} However imaging on the scale of single particles is considerably more challenging.

One powerful technique is confocal microscopy with fluorescently tagged particles. While there are significant materials limitations (refractive index of particles and the two fluids must all be matched; particles must be roughly 1 μm in diameter or larger), if these limitations can be managed, high-quality structural information at the particle scale can be obtained.^{18,25,26} An alternative is to use polymerizable oils, an approach that has been used to realize core-shell particles or solid bijels by polymerizing the particle-stabilized structure.^{6,13,27,28} Finally, it is possible to conduct electron microscopy on quenched samples under cryogenic conditions.^{28–34} Although cryo-electron microscopy is experimentally challenging, this method has the advantage that it can be applied with most pairs of fluids, and even with small particle sizes.

Here we report the first study of a newly developed ternary particle-liquid-liquid system which permits all three: structural characterization of the two-phase morphology, interfacial characterization at the scale of single particles, and detailed rheological characterization. The key idea is to use as the two immiscible fluids, not oil and water, but a pair of immiscible polymers, at least one of which is solid at room temperature. These polymers are blended under molten conditions at high temperature (with or without added particles), and then subjected to the desired flow history. The structure is quenched by simply cooling under quiescent conditions. Further structural characterization can follow various paths: transmission electron microscopy on microtomed samples if the particles are very small, optical microscopy if the particles are large, or in the present paper, selectively dissolving one polymer and using scanning electron microscopy (SEM). Since the interface can be imaged on the scale of single particles, questions such as what fraction of the interface is covered by the particles, are they well-ordered in a lattice or disordered, what is the contact angle of the particles, are the particles in a bridging configuration, can all be addressed. Furthermore, for the polymers chosen in this study, the melting temperature is sufficiently low that even extended rheological experiments are possible without thermal degradation. Furthermore the polymers are Newtonian fluids under experimental conditions allowing all non-Newtonian effects to be unambiguously attributed to interfacial phenomena.

In fact there have been numerous studies of interfacial adsorption of particles in two-phase polymeric systems. Much of this research was motivated by a desire to control the morphology and properties of blends of immiscible polymers. For example, the adsorption of carbon black at the interface can greatly increase the electrical conductivity of immiscible polymer blends.^{35–38} Adsorption of fumed silica, organically modified nanoclay platelets, or other nanoparticles at the interface can improve dispersion (*i.e.* lead to a two-phase morphology with a smaller length scale), prevent coalescence of drops, or prevent structural coarsening by jamming the interface.^{14,21,31,32,39–43} These and other related effects of interfacially adsorbed particles in polymeric systems have been reviewed thoroughly by Fenouillot *et al.*⁴⁴ The chief difference between the current research as compared to these past efforts on immiscible polymer blends is that we use monodisperse spherical particles with precisely controlled surface chemistry. This offers two major advantages. First, the location of the particle on the interface – in particular which phase is the preferentially wetting phase – is

unambiguously known. This is immensely useful in interpreting the observed structural and rheological consequences of particle addition. Second, at the volumetric loadings of ~ 1 vol% examined here, the particles – on their own – do not significantly affect the rheology. Thus all changes to the structure and rheology can be unambiguously attributed to the interfacial activity of particles and not to their mere presence in the blend. In contrast, when nanoclays, fumed silica, carbon black are used, they can affect the bulk rheology even at low volume fractions because of their high aspect ratio, fractal-like shape, or interparticle attractions.

This paper describes the effect of adding a small quantity of particles to droplet/matrix morphologies of two immiscible polymers. We show that particles can have a large effect on the drop sizes even at volume fractions under 0.1%. Furthermore, the contact angle of the particles has a tremendous effect on the morphology, in particular, when the particles are preferentially wetted by the continuous phase, they bridge across drops. The resulting drop clustering is then the dominant feature of the morphology. We also report on the gel-like linear viscoelastic properties of such bridged emulsions; a detailed rheological study will be published separately.

2. Materials and methods

Polyethylene oxide (PEO), M_w 20 000, (Fluka), and polyisobutylene (PIB), M_w 2200, (Soltex, USA) was used for all experiments. Monodisperse silica particles were synthesized using Stober's method as follows. 2850 ml ethanol (anhydrous, ACS/USP grade, Pharmco Products Inc.) was mixed with 300 ml of NH_4OH (28–30%, J.T.Baker) and stirred for 2 minutes. A mixture of 150 ml of ethanol and 75 ml of tetraethoxysilane (TEOS) was then added slowly, and the reaction continued for 24 h with continuous stirring to form silica particles. The particles were washed three times with ethanol with intermediate centrifugation steps to remove traces of NH_4OH . The size of the particles was measured using ZetaPALS, Brookhaven Instruments Corporation, and found to be 487 nm. The surface of the silica particles was hydrophobized using either octadecyltrichlorosilane (OTS) or dimethyldichlorosilane (DCDMS), both purchased from Gelest Inc., USA. The silica particles were first suspended in toluene and then the silane was added in excess to ensure hydrophobization. The mixture was stirred overnight to complete the silanization reaction. After the reaction, particles were washed 3 times with toluene (with centrifugation in between) to ensure removal of unreacted silane from the mixture. The hydrophobized silica was then dried at 80 °C overnight in an oven. The surface energy of these particles may be estimated to be 39–44 mN m^{-1} for DCDMS-modified silica,⁴⁵ and 20–24 mN m^{-1} for OTS-modified silica⁴⁶ (which is comparable to value specified by the supplier, Gelest, Inc.). The surface tensions of the two fluids are roughly 42 mN m^{-1} for the PEO under molten conditions⁴⁷ and 32 mN m^{-1} for the PIB.⁴⁶

The two polymers and silica were blended together in a Minimax mechanical mixer which resembles the parallel plate geometry of a rheometer, except that three ball bearings are added to ensure good mixing.⁴⁸ The blends were prepared in two steps: in the first step, the particles were dispersed into the continuous phase (PIB) at room temperature for 2 minutes at a rotational speed of 200 rpm. Then the mixing cup was opened

and the sample was briefly mixed by hand using a spatula. The cup was closed and mixing continued at 200 rpm for 1 min. The hand mixing is important because although the mixer can generate high stresses for dispersive mixing, its capabilities for distributive mixing are limited. Thus, without the hand-mixing step, there would generally be a portion of sample in the center of the cup that was not well-mixed. The particle containing PIB was observed under optical microscope to verify that there were no large aggregates visible. Occasionally a few particles aggregates were found even after mixing for longer time. In the second mixing step, the cup was heated to 80 °C, dispersed phase (PEO) added, and blended at a stirrer speed of 200 rpm for 2 min. The blends, which have the form of white viscous fluids, were then cooled, removed from the cup, and stored in plastic petridishes.

Blends were designated as E_{x-y} where “E” represents the dispersed phase (PEO), x is the weight percent of PEO (15, 25, 35, or 45) on a particle-free basis, and y is weight percentage of particles in the blend rounded to the nearest 0.01%. Almost all the results in this paper refer to OTS-modified particles, and hence the sample designation does not mention the silane used. In the few cases in this paper when unmodified or DCDMS-modified particles were used, it will be noted explicitly. The compositions of the various blends studied here are shown in Table 1 and in the composition diagrams of Fig. 2.

The blends were sheared in a controlled stress rheometer (AR 2000, TA Instruments) at 80 °C using a cone and plate geometry with 1° cone and a diameter of 40 mm. The sample was pre-sheared at a stress of 250 Pa, and then shearing was continued at a stress of 50 Pa for 2000 strain units. At the end of this shearing, the linear viscoelastic properties were measured. The entire shear history, which also includes of additional recovery and oscillatory steps, is illustrated in Fig. S1.† This paper will only discuss the morphology and viscoelastic properties at the end of the shearing process.

After the desired shear history, the blend was cooled to room temperature, and then cooled further to –35 °C for 15 minutes to ensure rapid and complete crystallization of the dispersed phase

Table 1 Compositions of the blends used in this paper

Sample id	Weight percentages			PEO : PIB weight ratio	Vol% particle ^a
	PEO	PIB	Particles		
E45-0	45.0	55.00	0	45 : 55	0.00
E45-2.25	43.9	53.76	2.25		1.02
E35-0	35.00	65.00	0	35 : 65	0.00
E35-0.07	34.98	64.95	0.07		0.03
E35-0.18	34.94	64.89	0.175		0.08
E35-0.35	34.88	64.77	0.35		0.16
E35-0.8	34.69	64.43	0.875		0.40
E35-1.7	34.39	63.86	1.75		0.81
E35-3.5	33.78	62.73	3.5		1.63
E25-0	25.00	75.00	0	25 : 75	0.00
E25-1.2	24.69	74.06	1.25		0.59
E15-0	15.00	85.00	0	15 : 85	0.00
E15-0.15	14.98	84.87	0.15		0.07
E15-0.35	14.95	84.70	0.35		0.17
E15-0.75	14.89	84.36	0.75		0.36
E15-1.75	14.74	83.51	1.75		0.84

^a Volume fraction calculated assuming silica particle density of 2.2 gm ml^{-1} , PIB density of 0.89 g ml^{-1} , and PEO density of 1.08 g ml^{-1} .

PEO. The rheometer was then brought back to room temperature, and the sample removed and stored for further study.

The blend morphology was examined by SEM and by optical microscopy. The optical images were obtained on blends that were extracted from the rheometer with no further sample treatment, and a few sample images are shown in ESI, Fig. S2 and S3.† These images are broadly consistent with the SEM images, except that the SEM images also show particle-scale details. Accordingly, only SEM images will be shown here. SEM imaging requires removing the continuous phase PIB. The blends were placed in sample vials and *n*-octane was added to dissolve PIB overnight. The PEO dispersed phase then formed a solid sediment which was pipetted drop wise on a Millipore 1 μm pore filter paper. A few drops of octane were then dripped over the filter to wash the PEO solids and ensure that no residual PIB remained on the filter paper. The filter paper was transferred to a carbon taped SEM stub, and coated with palladium using sputter coater for 120 s prior to SEM.

3. Results

3.1. Effect of particle surface modification on blend morphology

The first goal is to establish that the particles do indeed adsorb at the interface, that the chemical modification of the particles influences the particle wettability, and that changes in particle wettability influences the morphology of the blends. Four different polymer blends were prepared, all at a PEO : PIB ratio of 35 : 65, one without particles (the control case), and the remaining three with 0.35 wt% particles. Three different particle surfaces were compared: unmodified silica, OTS-modified, and DCDMS-modified silica. Fig. 3 shows the SEM images of the PEO drops. (Even though the PEO has solidified, we will nevertheless use the term “drops” to describe them. The term “particles” will be reserved to describe the silica particles.) Particles are evident at the interface in all three cases, but there are also clear differences. The most obvious difference is in contact angle: the OTS particles are

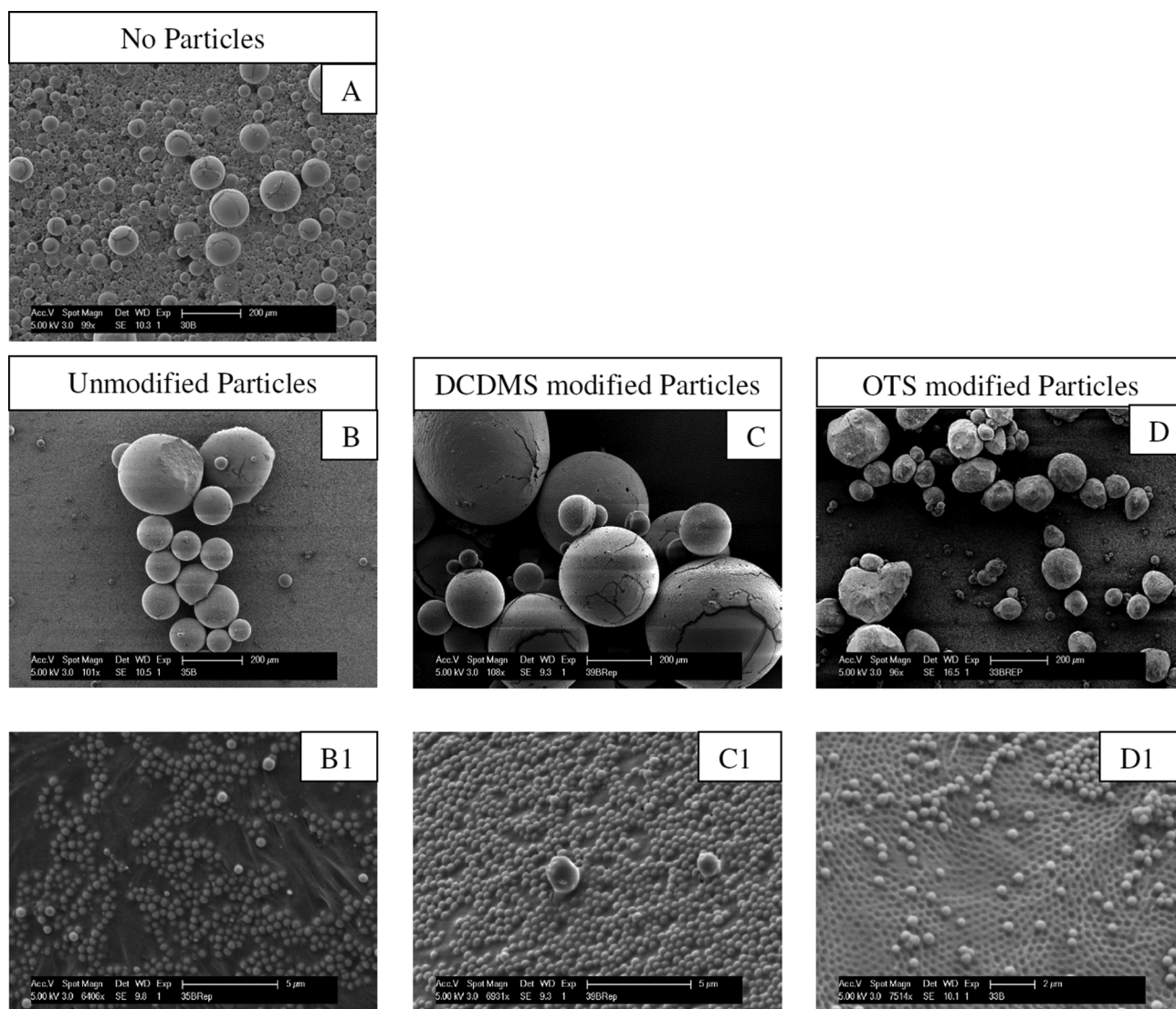


Fig. 3 Effect of particle addition on morphology of blends with a PEO : PIB weight ratio of 35 : 65, and 0.35 wt% particles of various surface modifications. Images (A–D) are on the scale of the PEO drops, whereas B1, C1 and D1 are on the scale of particles.

preferentially wetted by the PIB phase and hence protrude extensively outside the PEO drops. Indeed many of the OTS particles have debonded from the interface leaving craters. The diameter of these craters (estimated to be about 110 nm from analysis of about 50 craters using ImageJ image analysis software) allows an estimate of $\sim 150^\circ$ as the contact angle of the particles with respect to the PEO phase. In contrast, the DCDMS particles sit roughly symmetrically on the interface and do not debond. In this case it is more difficult to assign a contact angle, but image analysis suggests that the visible diameter of the particles is close to the measured particle diameter of 487 nm suggesting contact angle near 90° . Finally, in the case of the unmodified particles, an even smaller portion of the particle appears visible suggesting that the contact angle may be less than 90° . Furthermore, the interfacial coverage of the unmodified particles is also lower suggesting that some may have crossed the interface and desorbed inside the drop.

Fig. 3 also reveals large differences in the drop-scale morphology. In all cases, the addition of particles increases the drop size suggesting that addition of these particles promotes coalescence in these blends. The effects are especially dramatic for the DCDMS-modified and the unmodified particles in which case the largest drops are well over 200 μm in diameter. This drop dimension is comparable to the 300 μm gap at the edge of the cone and plate geometry, *i.e.* with these particles, the drops may possibly have grown even larger if not constrained by the flow geometry. The OTS particles also induce a drop size that is larger than the particle-free blend, and this will be examined experimentally in the following section.

The idea that addition of particles can promote coalescence has been well known in the aqueous foams literature for decades.^{49–51} The mechanism is believed to be “bridging–dewetting”: when a particle that is preferentially wetted by the dispersed phase simultaneously adsorbs onto two bubbles, the contact line recedes across the particle (*i.e.* dewets) and promotes coalescence. The same mechanism can be active in emulsions. Indeed an earlier article from our group had shown such particle-induced coalescence in polymer blends.²¹

However, the bridging–dewetting mechanism requires that the particle be preferentially wetted by the dispersed phase. If the particle is instead preferentially wetted by the continuous phase, bridging does not lead to dewetting, instead a stable bridge is formed that prevents coalescence.^{15–17} Indeed previous results on oil–water Pickering emulsions showed that with such stable bridging, two drops can be bridged by a tightly packed monolayer which can be extremely effective at stopping coalescence.^{18–22} In contrast, the results of Fig. 3 show all the particles, even the OTS-modified particles which are preferentially wetted by the continuous phase, can promote coalescence – an observation that to our knowledge has never been made. This will be discussed further later in this paper.

The final observation from Fig. 3A–C concerns the shapes of the drops. Most of the drops in Fig. 3A–C appear spherical and smooth; only the largest may be slightly deformed due to the confinement effect of the shear flow geometry. In contrast, the drops in Fig. 3D have distinctly irregular shapes, some with flattened regions. A glance at the optical image of this sample (ESI, Fig. S2D†) shows that while the dispersed phase morphology is similar to that shown in Fig. 3D, in fact prior to sample dissolution, the PEO drops were not individual separate

drops, but instead clusters that are substantially flattened in the region where drops touch each other. Further evidence of clustering comes from ESI Fig. S4B† which shows an SEM image of the same sample but at a different magnification. The appearance of these clusters is somewhat similar to aggregates of polyhedral foam bubbles. During the washing process, these clusters fall apart and it is these flattened regions that make the drops appear irregular. In the following section we will show that the clustering and flattening corresponds to regions where two drops are bridged together by a monolayer of particles.

The remainder of this paper focuses on OTS-coated particles and examines the interplay between bridging and jamming, and how these features control the morphology as the composition is changed. The unmodified or DCDMS-modified particles are not discussed in detail further in this paper.

3.2. Effect of OTS-modified silica particle loading

The effect of particle loading was examined for the E35-*y* and E15-*y* blends for OTS-modified particle loadings ranging from 0.07 to 3.5 wt%. Since each of these series of blends has a fixed PEO : PIB ratio, they correspond to the two blue dotted lines indicated by “increasing particle loading” in Fig. 2. The trends are broadly consistent for both series and hence only the E35-*y* series will be discussed here. The corresponding drop sizes, shapes, and surface features are shown in Fig. 4.

It is immediately evident that the trend in drop size is not monotonic with particle loading, a trend that to our knowledge has not been reported in the literature previously. Experiments with DCDMS particles (not discussed here) show similarly non-monotonic behavior. In the case of OTS-modified particles, addition of a small amount of particles, 0.07 wt% (Fig. 4B) or 0.18 wt% particles (not shown), causes a significant increase in drop size as compared to the particle-free blend. Increasing the particle loading beyond 0.35 wt% reduces the drop size. Along with the decrease in drop size, the drop shape changes as well from being predominantly spherical and smooth to increasingly irregular.

The particle-scale images of the interface give further insight. At low particle loadings, the particles are not uniformly distributed on the surface. The regions that appear smooth and spherical are essentially particle free, whereas the particles appear concentrated in discrete patches on the surface. Within these patches the particles are tightly crowded and show hexagonal close packing, at least over short distances. Thus, based on the optical images and the SEM images it is clear that the particle patches correspond to bridged monolayers, *i.e.* prior to sample dissolution, drops were glued together *via* these particle patches; during dissolution, the glued drops fell apart with each drop retaining either the particles, or craters.

As particle loading increases, the extent of particle bridging increases sharply until the drops show flat facets (Fig. 4C1). With further increase in particle loading (Fig. 4D1 and E1), there are no significant particle-free regions on the drop surface at all and the drop surfaces are jammed and unable to relax.

3.3. Effect of dispersed phase fraction

Returning to Fig. 2 we now trace a different path on the ternary composition diagram: varying drop loading while particle

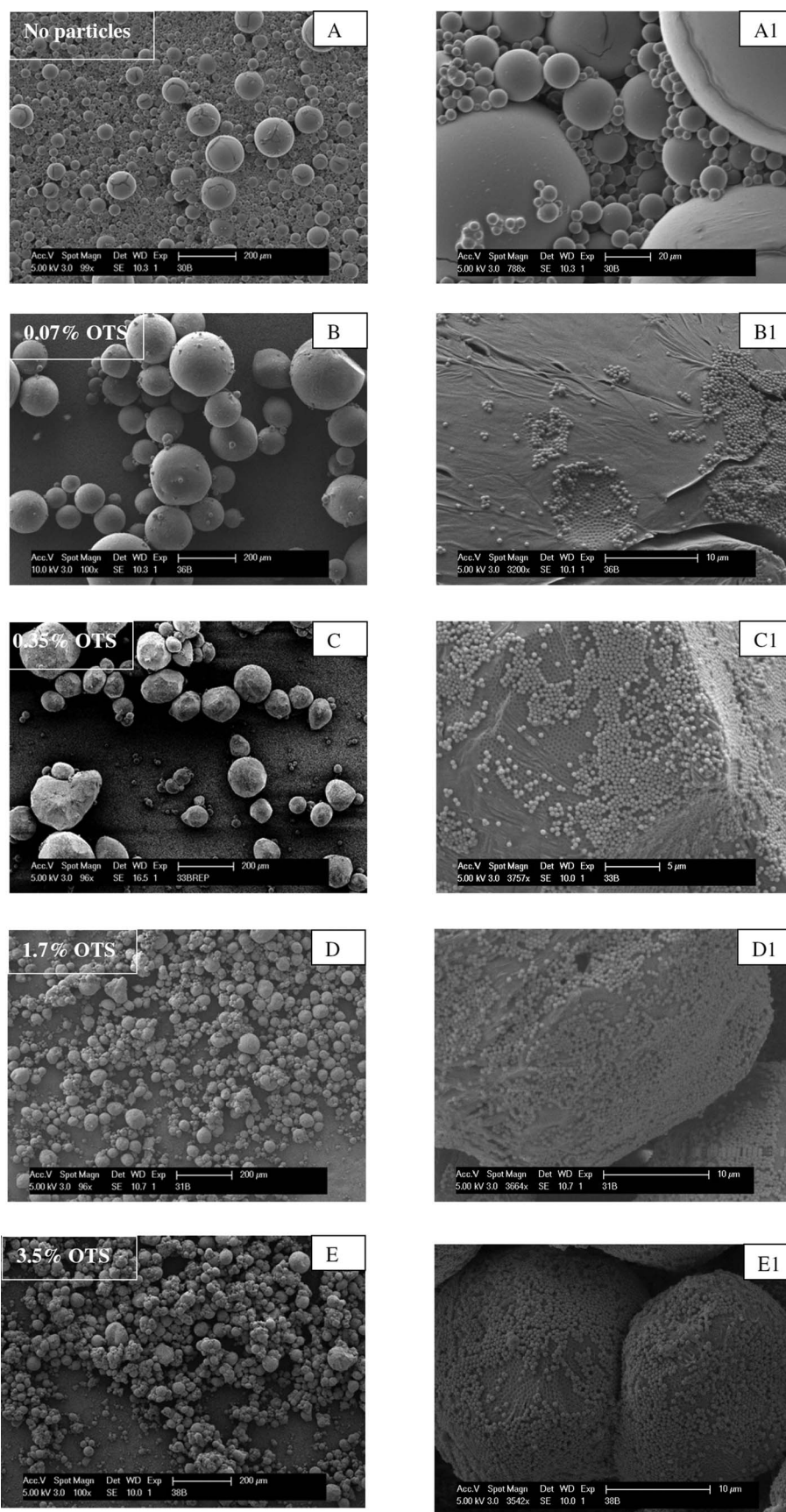


Fig. 4 The effect of OTS-modified silica particle concentration on morphology of E35- γ blends. The left column is at a low magnification to illustrate the drop-scale structure whereas the right column is on the scale of the particles.

loading is kept fixed. This was done at two particle loadings: 0.35 wt% and 1.75 wt%. These paths are illustrated by the two solid green horizontal lines marked “increasing dispersed phase”, and the corresponding SEM images are in Fig. 5.

At the lower particle loading of 0.35%, the E15-0.75 blend (Fig. 5A and A1) shows clear evidence of bridging-induced clusters. However the drops at the surface of these clusters still appear to have particle-free regions, and hence these outer drops in the cluster appear spherical. With an increase in

dispersed phase loading to 35%, (Fig. 5B) the drop size increases sharply, but also the particle coverage is significantly higher. The increased drop size likely reflects a higher coalescence rate due to the higher drop volume fraction: as the drop size increases, the particle coverage increases simply due to the reduced surface area. As remarked above, these drops are no longer spherical.

At the higher particle loading of 1.75%, the E15-1.75 blend (Fig. 5C) already shows drops with a high particle coverage at the

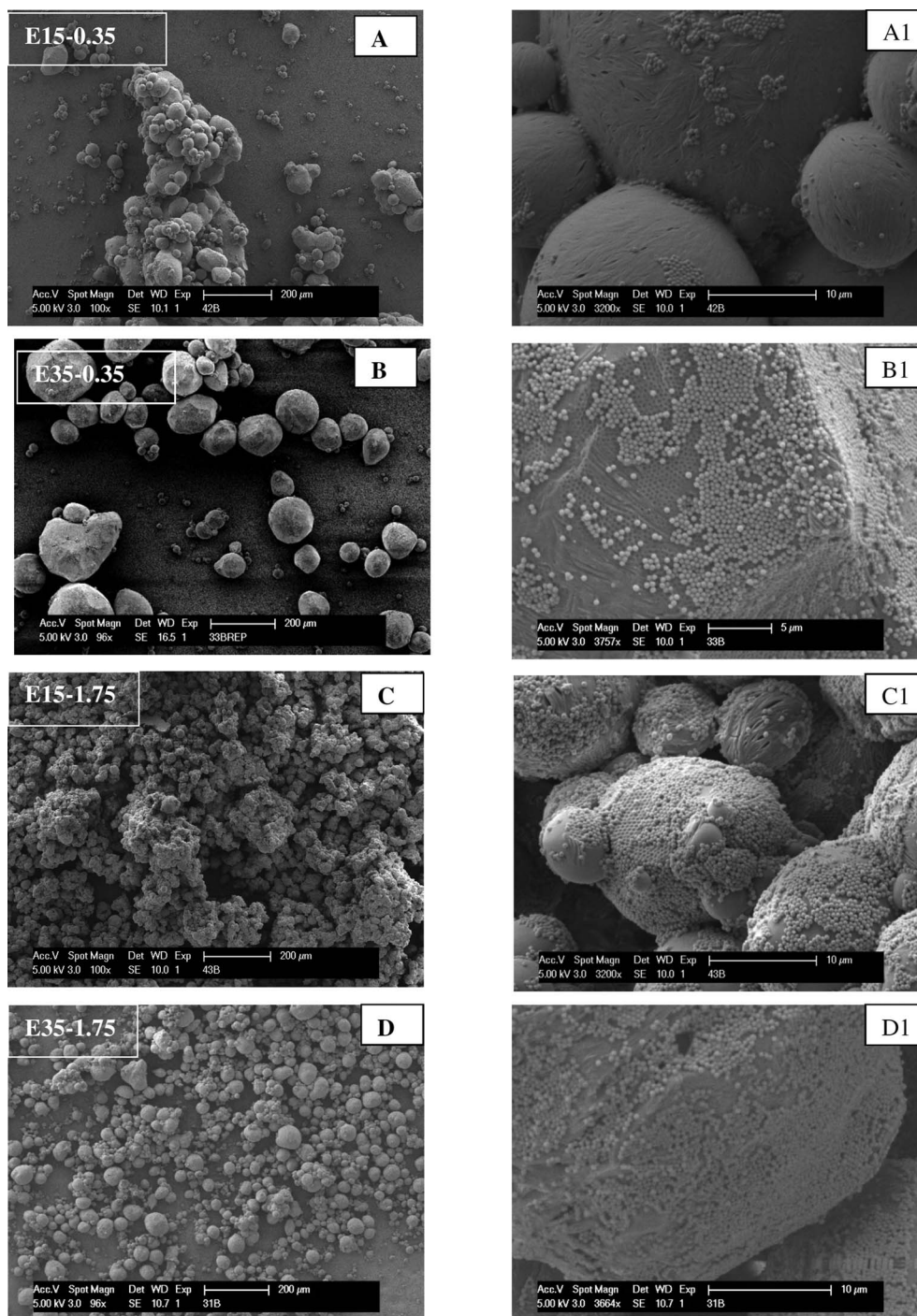


Fig. 5 Effect of dispersed phase loading at two different particle loadings of 0.35% (A and B) and 1.75% (C and D). Images in the right column are at higher magnification.

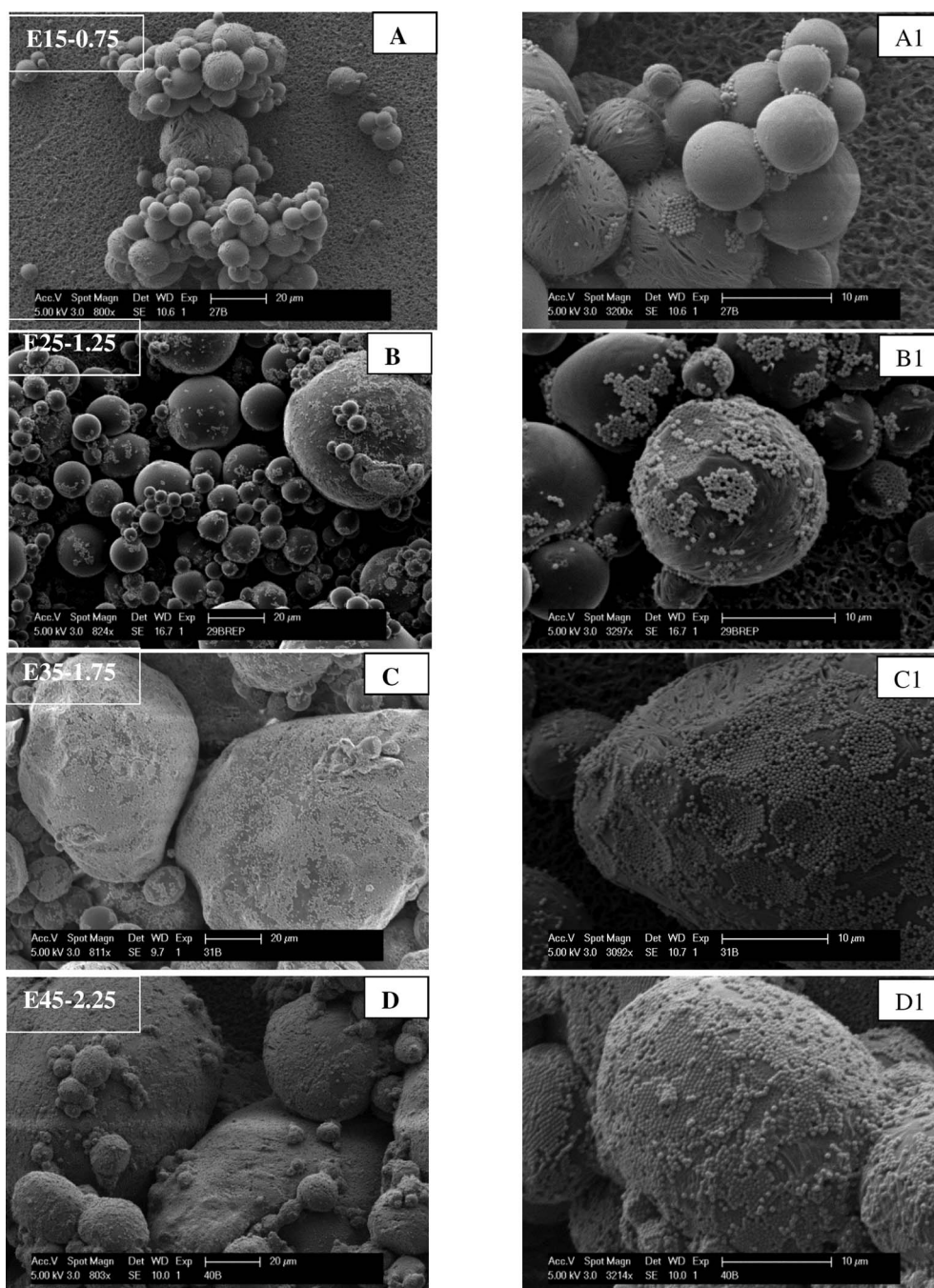


Fig. 6 Effect of continuous phase weight fraction on keeping particle : PEO ratio fixed. Images in the right column are at higher magnification. The scale bar is 20 μm for (A–D) and 10 μm for (A1–D1).

interface, *i.e.* since the particle loading is substantially higher than E15-0.35, the interfacial coverage is correspondingly larger and the drop size is smaller. The effect of increasing drop volume to $\sim 35\%$ is similar to before: the drop size increases with increasing drop volume fraction.

3.4. Effect of continuous phase volume fraction

The final trajectory on the ternary diagram considered here is to vary the amount of continuous phase while keeping the particles and the dispersed phase at nearly fixed weight ratio of 1 : 20. This

is illustrated by the red dashed diagonal line marked “increasing continuous phase” in Fig. 2B, and the corresponding images are shown in Fig. 6. In this case, since the particle loading changes proportionately to the PEO loading, the effects on the drop size, particle surface coverage and clustering are all expected to be a combination of the previous two sections. This is borne out experimentally. Fig. 6A, which corresponds to the largest amount (~ 85 wt%) of PIB continuous phase in this series, shows a morphology consisting of clusters of relatively small (less than 20 μm) drops, and the particles accumulate in bridging patches leaving much of the drop surfaces bare. As the amount of PIB is

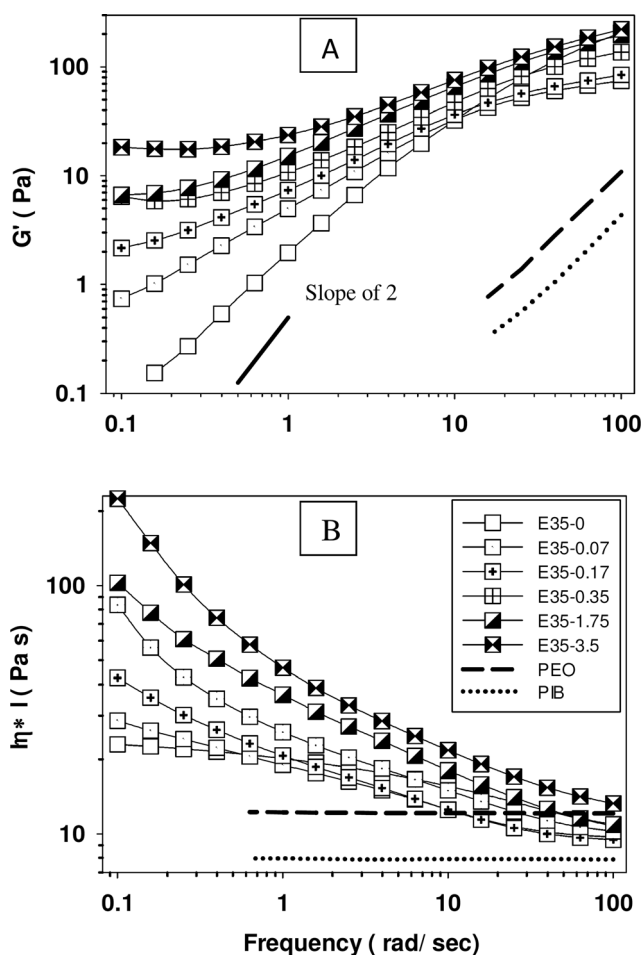


Fig. 7 Effect of particle loading in the E35- y blends on (A) magnitude of the complex viscosity and (B) storage modulus.

reduced, three effects are evident (1) the drops become larger (coalescence accelerates due to increasing particle content and due to increasing drop fraction), (2) the surface coverage increases (due to increasing particle content and decreasing surface area), and (3) the drops become increasingly bridged into clusters.

3.5. Small angle oscillatory experiments

The large changes in morphology described above are expected to result in corresponding changes in flow behavior. In this paper we will only examine linear viscoelastic properties measured by small-amplitude oscillatory experiments conducted immediately prior to quenching the morphology. Therefore the rheological behavior discussed in this section corresponds to the exact same dispersed phase morphologies discussed in Fig. 4–6.

Fig. 7 shows the effect of added particles on the linear oscillatory behavior of the ternary systems at a fixed PEO : PIB ratio of 35 : 65, *i.e.* following the line marked “increasing particle loading” in Fig. 2. These results were obtained immediately prior to quenching, *i.e.* they correspond to the linear viscoelastic properties of the dispersed phase morphologies of Fig. 4. The pure PEO and PIB show approximately Newtonian behavior

under these conditions, with the storage modulus G' being significantly lower than the loss modulus G'' . When the two fluids are blended together without particles (E35-0), the resulting blend shows a new relaxation mode manifested by a large increase in G' and a higher terminal viscosity $|\eta^*|$. Such viscoelasticity arising when two immiscible fluids are blended together is very well-known and is attributable to the contribution of the interface to the rheology.^{52–55} Briefly, at high oscillation frequency, the drops are not able to relax to their spherical shapes and hence the deformation of the interface gives rise to an elastic response. If the oscillation frequency is relatively low, the drops maintain their spherical shapes during the oscillation and the elastic response is diminished. It is crucial to note that this blend is still liquid-like: at low frequency, the G' varies roughly with the square of the frequency, and the magnitude of the complex viscosity shows a clear plateau whose value is the terminal complex viscosity.

Upon addition of particles, there is an increase in the magnitude of the complex viscosity as well as the storage modulus at all frequencies. Indeed, there is a qualitative change in behavior: at low frequencies, the storage modulus G' shows a plateau, and the magnitude of the terminal viscosity $|\eta^*|$ appears to diverge, both indicative of solid-like or gel-like behavior. The apparent solid-like behavior becomes progressively stronger as particle loading is increased. Such solid-like behavior of particle-stabilized emulsions has been seen reported previously,^{18,20,21,30} and will be discussed further in Section 4. It must be noted that the rheological results at low particle loadings are not highly reliable since the previous section showed that drop size is comparable to the shear gap, thus, the results are likely influenced by the measurement geometry. For particle loadings exceeding 0.35 wt%, the drop sizes are significantly smaller than the geometry and the rheological results may be considered to be reliable.

Fig. 8, shows the effect of drop loading keeping particle loading fixed (horizontal line marked “increasing dispersed phase” on the ternary diagram of Fig. 2). The corresponding morphologies were shown in Fig. 5. It is clear that the gel-like behavior becomes more pronounced (*i.e.* the plateau in G' at low frequency increases) with increasing dispersed phase loading. This is true at both the particle loadings examined. In the E15-0.35 blend, a clear plateau in G' is not evident at low frequency. Nevertheless, there is still a large increase in G' over the corresponding particle-free blend E15-0, and liquid-like scaling ($G' \propto \text{frequency}^2$) is not evident even at the lowest accessible frequency. It is crucial to note that all these blends – even the E15-0.35 blend – show significant bridging-induced clustering. These results simply indicate that the clustering does not produce a clear plateau in G' at low frequencies unless the drop loading is sufficiently high.

Finally Fig. 9 follows the dashed line trajectory labeled “decreasing continuous phase”, corresponding to the morphological trends of Fig. 6. As mentioned previously, this corresponds to increasing the particle and drop loading simultaneously while maintaining a particle : dispersed phase ratio of approximately 1 : 20. Since both particle loading and drop loading enhance gel-like behavior, not surprisingly, the G' and $|\eta^*|$ at low frequency both increase sharply as the continuous phase volume fraction reduces.

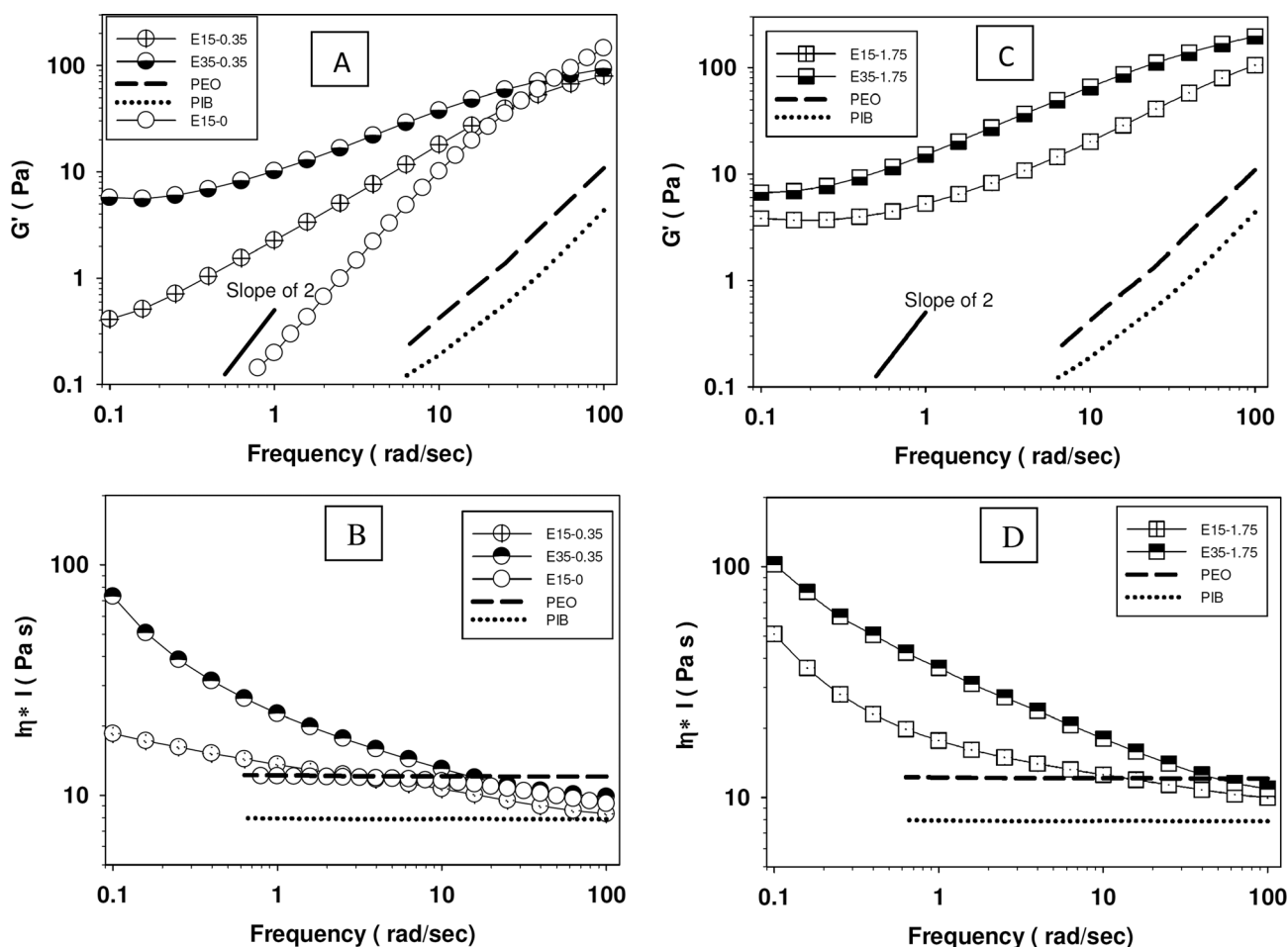


Fig. 8 Effect of dispersed phase loading on the rheology of blends with 0.35 wt% particles (A and B) and 1.75 wt% particles (C and D).

4. Discussion

Here we will first summarize the morphological picture that arises from the experimental results and then discuss the rheological behavior. The added particles appear to have three microstructural effects.

(1) The OTS-coated silica particles, like other interfacially active particles, adsorb almost irreversibly on the interface. Therefore they are capable of jamming the interface if the interfacial coverage is sufficiently large.^{2,8-14}

(2) Being preferentially wetted by the continuous phase, particles can also bridge across two drops and induce drop clustering. Bridging can occur at all particle loadings, high as well as low. Furthermore, the bridging interaction is strong: Appendix I presents scaling arguments suggesting that at the stress level of 50 Pa applied here, even a single particle bridge is sufficient to hold together two drops that are a few-microns in diameter. A multi-particle bridge is likely to be even stronger and hold even larger drops together. Thus if drops are roughly 10 microns in diameter or smaller, the bridging interaction is nearly irreversible: the applied stress is not large enough to pull small drops off clusters or to break apart small clusters. Bridging clusters can be broken of course, but this can occur only when the individual drops in a cluster grow to a large size, or when the cluster itself grows sufficiently large. For these reasons, bridging profoundly

influences the morphology of the ternary system. It is important to note that due to the solvent treatment prior to SEM, not all the SEM images show extensive clustering. Nevertheless all optical images of blends containing OTS-coated particles show significant clustering, and in fact clusters are present at all loadings. Indeed one very recent article that used confocal imaging on an index-matched oil-water system has shown polyhedral drop cluster morphologies that are similar to the clusters shown in Fig. S2 and S3,[†] albeit at far higher particle loadings.¹⁸

(3) Finally, the particles are also able to promote coalescence, especially at low particle loadings.

The net morphology then is a competition between these three effects, and which of these effects are active depends on the particle loading.

When the particle loading is low, the particles induce the drops to cluster, and the particles preferentially accumulate in the bridging region between the drops (Fig. 10A). Since the rest of the drop surface is particle-free, the drops – at least those at the surface of the cluster – are mostly spherical. The bridged patch is significantly flattened, and in some cases the bridged region on large drops appears as a dimple. Particularly clear examples of such concave dimples are seen in Fig. 6B1 and C1 and 4B1. Such concavity is likely associated with the capillary pressure: the capillary pressure inside the drops is inversely proportional to the curvature of the spherical portion of the drop, and hence smaller

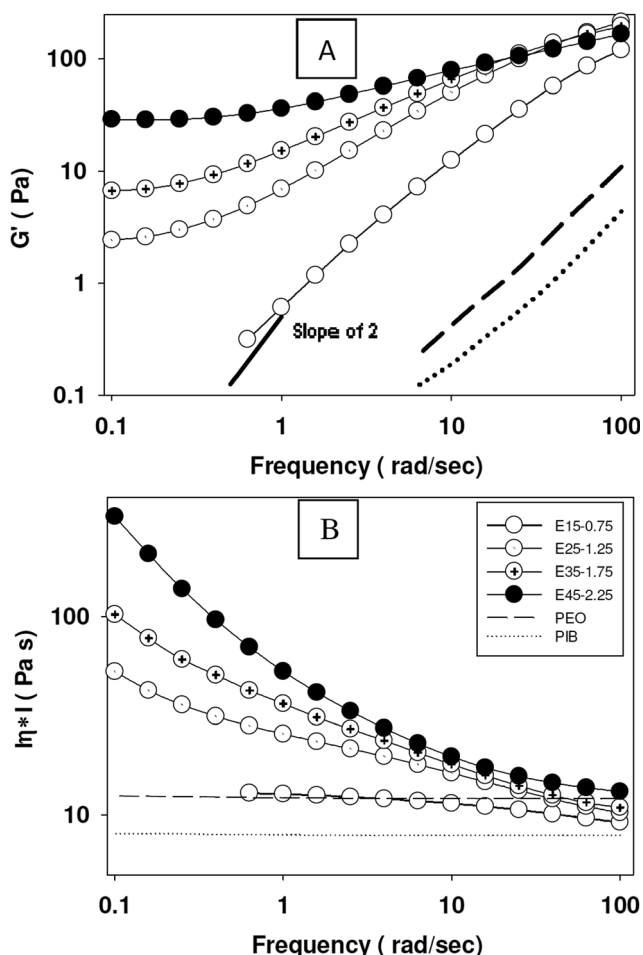


Fig. 9 Effect PIB dispersed phase loading on the rheology of blends at a fixed particle : PEO ratio.

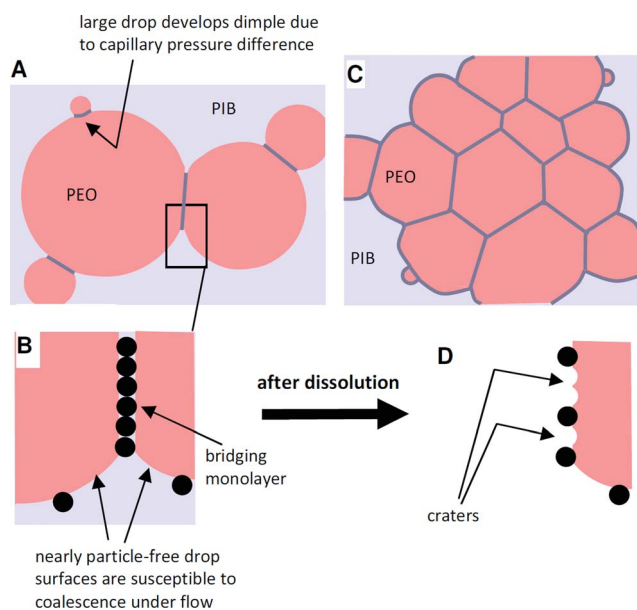


Fig. 10 Schematic structure of the particle-containing polymer blends at (A) low particle surface coverage, and (C) at high surface coverage. (B) Illustrates the structure of the bridging monolayer. (D) Shows that when the cluster debonds, the some particles debond leaving craters.

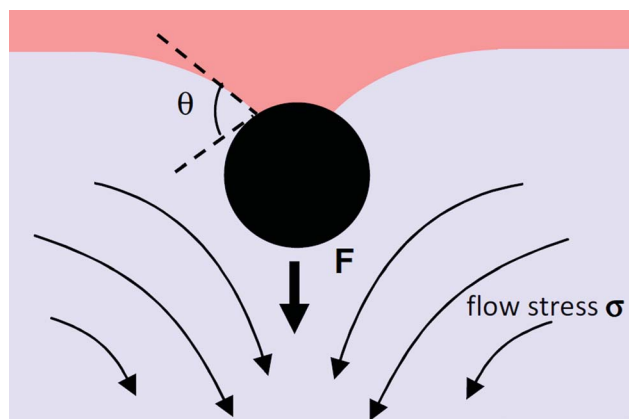


Fig. 11 A particle adsorbed at an interface experiencing a flow field at a typical stress of σ normal to the interface. The meniscus deforms holding the particle on the interface until at some maximum value of force F_m , the particle is pulled off the interface (see Appendix text).

drops are expected to have a significantly higher capillary pressure. Thus when a small drop bridges with a large drop, the interface is expected to be concave with respect to the large drop as illustrated in Fig. 10A.

Under these circumstances of low particle coverage, particles promote coalescence under flow conditions. As mentioned in Section 3.2., particle-induced coalescence is well-known, but the corresponding bridging-dewetting mechanism^{49,50} is physically meaningful only if the particles are preferentially wetted by the drop phase. When particles are preferentially wetted by the continuous phase, the bridges are expected to be stable, and indeed at least two authors^{18,19} have confirmed that tightly packed bridging monolayers, very similar to those seen in this paper, do stabilize drops. Why then do our results show that OTS particles, which are preferentially wetted by the continuous phase, promote coalescence? We speculate that if the drop surface is not completely covered with particles, the edge of the bridged monolayer is susceptible to coalescence; this is because the two drops are held in close proximity, but their surfaces are not protected by particles as illustrated in Fig. 10B. Accordingly, the thin region of continuous phase immediately outside of the bridged monolayer can rupture allowing coalescence to proceed. Under quiescent conditions, coalescence does not proceed at a significant rate, but under flow conditions, there is sufficient disturbance in the edge region to rapidly promote rupture and drop coalescence. Only when the entire drop is completely covered with particles does the region outside of the bridging monolayer become immobile, causing coalescence to be suppressed. These experiments may therefore highlight a difference between quiescent coalescence vs. flow-induced coalescence: in the former, a bridged monolayer alone is sufficient to stop coalescence;¹⁹ in the latter a bridged monolayer is not sufficient; near-complete coverage of the entire interface is necessary.

At high particle surface coverage (either because of increased particle loading, or because of decrease in interfacial area due to faster flow-induced coalescence), the morphology may be schematically represented by Fig. 10C: the clusters are large and the drops on the interior of the cluster are polyhedral. Typical examples include Fig. S2D and S6D.† In this case, there are few particle-free surfaces: the inner and outer surfaces of the clusters

all have a relatively high particle coverage. Indeed Lee *et al.*¹⁸ have very recently noted a foam-like structure, which they dubbed “Pickering gels”, composed of polyhedral bridged drops, although their particle loadings were much higher (8–17 vol% as compared to ~1 vol% in this paper). Finally, in this context, it is also relevant to mention the work of Fujii *et al.*^{5,56} which also shows a polyhedral foam resulting from particle adsorption, however, in that case the bubbles are not bridged by a particle monolayer, but instead by a bilayer of singly adsorbed particles.

Regardless of whether the surface coverage is high or low, our preparation protocol for SEM disrupts the cluster structure: some bridged clusters remain, but many fall apart. Accordingly the particles remain adhered to one of the drops leaving behind craters on the other; this was seen in numerous SEM images and is shown schematically in Fig. 10D.

A final comment on the morphology concerns the effect of stress. While this paper does not discuss effects of stress, we have conducted limited studies on how the stress affects the morphology. Broadly speaking, stresses that are significantly higher than that used here reduce the drop size, which in turn reduces surface coverage, *i.e.* in qualitative terms, lowering the stress is equivalent to an increase in particle loading. In fact, one extreme effect of stress is evident from Fig. S4A and S4A1† which examines the morphology as-blended (prior to the shear history of Fig. S2†). During the blending process, the stresses experienced in the mixer are far higher leading to a far smaller drop size, and hence a higher surface area (Fig. S4A and A1†). In this case, the drops are round, the particle coverage is low, and faceted regions are not evident – all sharply different from the same sample after shearing at 50 Pa.

These major changes in the morphology caused by addition of particles induce corresponding changes in the flow behavior. Most importantly, with addition of a sufficiently high particle loading, the flow behavior changes qualitatively from a liquid-like behavior to a solid-like behavior with a non-zero modulus at low frequencies. Such changes in behavior have been noted previously in particle–liquid–liquid systems.^{18,20,21,30} The existence of a low-frequency modulus is indicative of a large-scale, space-spanning (*i.e.* percolating) structure being present. The SEM images offer a clear picture of the nature of the percolating structure. At low surface coverage (*i.e.* at small particle loading), most of the drop surfaces are particle-free, and the particles are preferentially located in tightly packed bridging clusters. Since the volume of the drops is far larger than of the particles, the percolating structure may be regarded as being composed of approximately round drops adhering together *via* bridging patches. This is exactly the inverse of the pendular state (see Fig. 2A) in suspensions or granular systems:^{57,58} in that case the particles are present at a large volume fraction, and they are adhered together by a small volume of fluid located in capillary bridges between the particles. The resulting percolating structure induces a transition from free-flowing behavior to solid-like behavior, most familiar in the context of building sandcastles from moist sand, but also known in the case of suspensions.⁵⁹

At high surface coverages, not just the bridging region, but almost the entire drop surfaces appear to be covered by particles. The optical images suggest that the morphology somewhat resembles a foam structure – but with the interface covered almost

completely with particles. Thus, with a sufficiently high degree of clustering, the particles may form a percolating structure on their own. Indeed Lee *et al.*¹⁸ observed that in their samples (with particle volume fractions typically an order of magnitude higher than our samples), the rheology was primarily determined by particle loading (not by dispersed phase loading) strongly suggesting a percolating structure that was composed of particles only.

Our shear history allows other rheological behavior, in particular creep and creep recovery, to be measured. While these are not discussed in detail here, briefly, the viscosity of blends containing OTS-modified particles shows an overshoot during creep experiments which is indicative of breakdown of the gel-like structure. Additional experiments (*i.e.* using a shear history different from Fig. S1†) indicate that blends containing OTS-modified particles have a yield stress behavior, *i.e.* a stress below which viscosity rises sharply. Such viscosity overshoots or yield stresses are not evident in particle-free blends or blends containing DCDMS-modified particles.

A final comment concerns the nature of inter-particle attraction in these systems as compared to oil–water systems. In numerous oil–water systems it has been noted that monodisperse particles adsorbed at the oil–water interface repel each other and form two-dimensional lattices.^{60–62} This is attributable to Coulombic repulsion mediated through the oil phase.^{61,63,64} In our experiment, we have not seen a single example of 2D lattice formation. We presume this is because both the polymers have relatively low polarity (as compared to water) and hence Coulombic repulsions, or indeed any other charge interactions, are weak.

5. Conclusions

In summary, this research has examined the role of interfacially active particles on the structure and rheology of immiscible polymer blends with a droplet–matrix morphology. Experiments were conducted at low particle loadings, with most experiments having less than 1 vol% of particles. The wettability of the particles was found to significantly affect the morphology: particles that are preferentially wetted by the continuous phase are able to bridge across drops. Thus the particles are not uniformly distributed on the interface, but instead preferentially accumulate in the bridge region between drops. The resulting drop clusters are a dominant feature of the morphology. Nevertheless, such particle bridging cannot stabilize drops against flow-induced coalescence, and hence at small particle loadings, the drops are larger than the particle-free blends due to particle-induced coalescence. Only when the surface coverage increases sufficiently high does the drop size reduce with an increase in particle loading. Rheologically, the chief effect of particles is to change the flow behavior from a free-flowing liquid-like rheology to solid-like or gel-like behavior. This liquid-like to solid-like transition appears to be analogous to the pendular state in granular or suspension systems, except that here the structure is composed of drops held together by particles rather than *vice versa*.

Perhaps the most important qualitative conclusion from this paper is that interfacially adsorbed particles can greatly influence the morphology and flow characteristics of liquid–liquid mixtures even at volumetric loadings of less than 0.1%. This is of

relevance to structure control in both polymer blends as well as oil–water systems.

6. Appendix I

Consider a particle of radius R_p adsorbed at an interface with the contact angle θ . If a force, F , is applied normal to the interface, the meniscus deforms so as to resist this force. The maximum force that can be resisted is¹⁵

$$F_m = 2\pi\alpha R_p \cos^2\left(\frac{\theta}{2}\right)$$

If the applied force exceeds this value, the particle will desorb off the interface.

Now consider a drop of radius R_d adhering to a flat interface with a single particle bridge. If a flow is applied as illustrated in Fig. 11 at a stress of σ , the viscous force on the drop scales as $\pi R_d^2 \sigma$. Equating this to F_m yields the largest drop size $R_{d,m}$ that can remain adhered to the interface in a flow at the specified stress level:

$$2\pi\alpha R_p \cos^2\left(\frac{\theta}{2}\right) = \pi\alpha R_{d,m}^2 \sigma$$

Solving the above equation, the maximum drop size $R_{d,m}$ is given by

$$R_{d,m} = \left(\frac{2\alpha R_p}{\sigma}\right)^{0.5} \cos\left(\frac{\theta}{2}\right)$$

The particle bridge cannot be sustained if the drop is significantly larger than $R_{d,m}$.

It is important to highlight the differences between the assumptions in the above estimate vs. the experimental situation: (1) the flow profile is shown as being normal to the interface, suggestive of an elongational flow, whereas the actual experiment is in shear flow (2) in the shear flow experiment, the more relevant situation is of two (or more) drops sticking to each other, rather than a single drop sticking to a flat interface. Therefore rotation of the cluster about the vorticity direction will make it more difficult to separate the drops. For these reasons, the value of $R_{d,m}$ calculated by the above approach is likely to be an underestimate.

With these caveats, we can estimate $R_{d,m}$ for our present experiment in which $R_p = 0.24 \mu\text{m}$, $\sigma = 50 \text{ Pa}$, and $\theta = 150^\circ$ can be estimated from the crater sizes in Fig. 3D1. The interfacial tension has not been measured, but is expected to be approximately 0.01 N m^{-1} as typical for polymer pairs.⁴⁷ This yields $R_{d,m} = 2.5 \mu\text{m}$ as the largest radius drop that can remain adhered by a single particle bridge. Note that this calculation is highly sensitive to the value of the contact angle: raising the contact angle to 160° reduces $R_{d,m}$ to $1.7 \mu\text{m}$. If multiple particles bridge the drop to the flat interface, $R_{d,m}$ would be higher.

The chief conclusion from this estimate is that the relatively small drops such as in Fig. 5C1 and 6A1 or 6B1, which are only a few microns in diameter but are held together by several particle bridges, are not likely to be pulled off in the applied flow. Instead, these drops are likely to remain clustered nearly irreversibly.

Clusters composed of large drops that are several ten microns in size are likely to be reversible, *i.e.* they may breakdown in shear flow. This is because the above analysis is not applicable if the bridging monolayer is very large in extent; in that case, the drops can separate by an edge peeling mechanism (analogous to peeling a tape from a substrate) in which unbridging occurs inwards from the edge of the bridging monolayer.¹⁵

Acknowledgements

This research was funded by NSF-CBET Grant #0932901. We are grateful to Dr Luling Wang and Prof. Sanford Asher for guiding the synthesis of the silica particles.

References

- 1 B. P. Binks, *Curr. Opin. Colloid Interface Sci.*, 2002, **7**, 21.
- 2 S. U. Pickering, *J. Chem. Soc., Trans.*, 1907, **91**, 2001.
- 3 W. Ramsden, *Proc. R. Soc. London, Ser. A*, 1903, **72**, 156.
- 4 P. Thareja, B. P. Ising, S. J. Kingston and S. Velankar, *Macromol. Rapid Commun.*, 2008, **29**, 1329.
- 5 S. Fujii, P. D. Iddon, A. J. Ryan and S. P. Armes, *Langmuir*, 2006, **22**, 7512.
- 6 R. Murakami and A. Bismarck, *Adv. Funct. Mater.*, 2010, **20**, 732.
- 7 B. P. Binks and R. Murakami, *Nat. Mater.*, 2006, **5**, 865.
- 8 H. L. Cheng and S. S. Velankar, *Langmuir*, 2009, **25**, 4412.
- 9 A. B. Subramaniam, C. Mejean, M. Abkarian and H. A. Stone, *Langmuir*, 2006, **22**, 5986.
- 10 K. Stratford, R. Adhikari, I. Pagonabarraga, J.-C. Desplat and M. E. Cates, *Science*, 2005, **309**, 2198.
- 11 M. E. Cates and P. S. Clegg, *Soft Matter*, 2008, **4**, 2132.
- 12 E. M. Herzig, K. A. White, A. B. Schofield, W. C. K. Poon and P. S. Clegg, *Nat. Mater.*, 2007, **6**, 966.
- 13 M. N. Lee and A. Mohraz, *Adv. Mater.*, 2010, **22**, 4836.
- 14 H. Chung, K. Ohno, T. Fukuda and R. J. Composto, *Nano Lett.*, 2005, **5**, 1878.
- 15 E. J. Stancik and G. G. Fuller, *Langmuir*, 2004, **20**, 4805.
- 16 N. P. Ashby, B. P. Binks and V. N. Paunov, *Chem. Commun.*, 2004, 436.
- 17 T. S. Horozov, R. Aveyard, J. H. Clint and B. Neumann, *Langmuir*, 2005, **21**, 2330.
- 18 M. N. Lee, H. K. Chan and A. Mohraz, *Langmuir*, 2012, **28**, 3085.
- 19 T. S. Horozov and B. P. Binks, *Angew. Chem., Int. Ed.*, 2006, **45**, 773.
- 20 P. Thareja and S. Velankar, *Rheol. Acta*, 2006, **46**, 405.
- 21 P. Thareja and S. Velankar, *Rheol. Acta*, 2008, **47**, 189.
- 22 J. Vermant, S. Vandebriel, C. Dewitte and P. Moldenaers, *Rheol. Acta*, 2008, **47**, 835.
- 23 S. Sacanna, W. K. Kegel and A. P. Philipse, *Langmuir*, 2007, **23**, 10486.
- 24 Y. Lin, H. Skaff, T. Emrick, A. D. Dinsmore and T. P. Russell, *Science*, 2003, **299**, 226.
- 25 A. D. Dinsmore, M. F. Hsu, M. G. Nikolaidis, M. Marquez, A. R. Bausch and D. A. Weitz, *Science*, 2002, **298**, 1006.
- 26 S. Tarimala and L. L. Dai, *Langmuir*, 2004, **20**, 3492.
- 27 A. Menger, R. Verdejo, M. Shaffer and A. Bismarck, *Langmuir*, 2007, **23**, 2398.
- 28 D. J. Voorn, W. Ming and A. M. van Herk, *Macromolecules*, 2006, **39**, 2137.
- 29 B. Madivala, S. Vandebriel, J. Fransara and J. Vermant, *Soft Matter*, 2009, **5**, 1717.
- 30 B. P. Binks, J. H. Clint and C. P. Whitby, *Langmuir*, 2005, **21**, 5307.
- 31 J. Vermant, G. Cioccolo, K. Golapan Nair and P. Moldenaers, *Rheol. Acta*, 2004, **43**, 529.
- 32 S. Vandebriel, J. Vermant and P. Moldenaers, *Soft Matter*, 2010, **6**, 3353.
- 33 E. Bourgeat-Lami, T. R. Guimaraes, A. M. C. Pereira, G. M. Alves, J. C. Moreira, J. L. Putaux and A. M. dos Santos, *Macromol. Rapid Commun.*, 2010, **31**, 1874.
- 34 M. Reger and H. Hoffmann, *J. Colloid Interface Sci.*, 2012, **368**, 378.

- 35 F. Gubbels, R. Jerome, P. Teyssie, E. Vanlathem, R. Deltour, A. Calderone, V. Parente and J. L. Bredas, *Macromolecules*, 1994, **27**, 1972.
- 36 F. Gubbels, R. Jerome, E. Vanlathem, R. Deltour, S. Blacher and F. Brouers, *Chem. Mater.*, 1998, **10**, 1227.
- 37 A. E. Zaikin, R. R. Karimov and V. P. Arkhireev, *Colloid J.*, 2001, **63**, 53.
- 38 M. Sumita, K. Sakata, Y. Hayakawa, S. Asai, K. Miyasaka and M. Tanemura, *Colloid Polym. Sci.*, 1992, **270**, 134.
- 39 L. Elias, F. Fenouillot, J. C. Majesté, P. Alcouffe and P. Cassagnau, *Polymer*, 2008, **49**, 4378.
- 40 L. Elias, F. Fenouillot, J. C. Majeste, G. Martin and P. Cassagnau, *J. Polym. Sci., Part B: Polym. Phys.*, 2008, **46**, 1976.
- 41 L. Elias, F. Fenouillot, J. C. Majeste and P. Cassagnau, *Polymer*, 2007, **48**, 6029.
- 42 W. Tong, Y. J. Huang, C. L. Liu, X. L. Chen, Q. Yang and G. X. Li, *Colloid Polym. Sci.*, 2010, **288**, 753.
- 43 S. Gam, A. Corlu, H. J. Chung, K. Ohno, M. J. A. Hore and R. J. Composto, *Soft Matter*, 2011, **7**, 7262.
- 44 F. Fenouillot, P. Cassagnau and J. C. Majeste, *Polymer*, 2009, **50**, 1333.
- 45 P. Thareja and S. S. Velankar, *Colloid Polym. Sci.*, 2008, **286**, 1257.
- 46 D. Janssen, R. De Palma, S. Verlaak, P. Heremans and W. Dehaen, *Thin Solid Films*, 2006, **515**, 1433.
- 47 S. Wu, *Polymer Interface and Adhesion*, Marcel Dekker, New York, 1982.
- 48 M. Maric and C. W. Macosko, *Polym. Eng. Sci.*, 2001, **41**, 118.
- 49 *Defoaming. Surfactant Science Series*, ed. P. R. Garrett, Marcel Dekker, New York, 1993.
- 50 P. R. Garrett, *Mode of Action of Antifoams, in Defoaming*, ed. P. R. Garrett, Marcel Dekker, New York, 1993.
- 51 T. N. Hunter, R. J. Pugh, G. V. Franks and G. J. Jameson, *Adv. Colloid Interface Sci.*, 2008, **137**, 57.
- 52 J. G. Oldroyd, *Proc. R. Soc. London, Ser. A*, 1953, **218**, 122.
- 53 J. F. Paliarne, *Rheol. Acta*, 1990, **29**, 204.
- 54 H. Gramespacher and J. Meissner, *J. Rheol.*, 1997, **41**, 27.
- 55 J. D. Martin and S. S. Velankar, *J. Rheol.*, 2007, **51**, 669.
- 56 S. Fujii, A. J. Ryan and S. P. Armes, *J. Am. Chem. Soc.*, 2006, **128**, 7882.
- 57 S. J. R. Simons and P. Pagliai, *High Temperature Granular Interactions, in Granular Materials: Fundamentals and Applications*, ed. S. J. Anthony, W. Hoyle and Y. Ding, Royal Society of Chemistry, Cambridge, 2004.
- 58 H. J. Butt, *Science*, 2011, **331**, 898.
- 59 S. Vankao, L. E. Nielsen and C. T. Hill, *J. Colloid Interface Sci.*, 1975, **53**, 367.
- 60 P. Pieranski, *Phys. Rev. Lett.*, 1980, **45**, 569.
- 61 R. Aveyard, J. H. Clint, D. Nees and V. N. Paunov, *Langmuir*, 2000, **16**, 1969.
- 62 E. J. Stancik, G. T. Gavranovic, M. J. O. Widenbrant, A. T. Laschitsch, J. Vermant and G. G. Fuller, *Faraday Discuss.*, 2003, **123**, 145.
- 63 B. J. Park, J. P. Pantina, E. M. Furst, M. Oettel, S. Reynaert and J. Vermant, *Langmuir*, 2008, **24**, 1686.
- 64 R. Aveyard, *et al.*, *Phys. Rev. Lett.*, 2002, **88**, 246102.
- 65 E. Koos and N. Willenbacher, *Science*, 2011, **331**, 897.